Real-Time Monitoring of Temperature-Dependent Structural Transitions in DNA Nanomechanical Resonators: Unveiling the DNA-Ligand Interactions for Biomedical

ACS APPLIED NANO MATERIALS

www.acsanm.org

Article

Real-Time Monitoring of Temperature-Dependent Structural Transitions in DNA Nanomechanical Resonators: Unveiling the DNA−Ligand Interactions for Biomedical Applications

Francesca Legittimo, Monica Marini, Stefano Stassi, Enzo Di Fabrizio, and Carlo Ricciardi*

Cite This: *ACS Appl. Nano Mater.* 2023, 6, 2249−2257

Read Online

ACCESS | Metrics & More | Article Recommendations | Supporting Information

ABSTRACT: Despite being widely recognized as of paramount importance in molecular biology, real-time monitoring of structural transitions in DNA complexes is currently limited to complex techniques and chemically modified oligonucleotides. Here, we show that nanomechanical resonators made of different DNA complexes, such as pristine dsDNA, ssDNA, and DNA intercalated with dye molecules or chemotherapeutic agents, are characterized by unique fingerprint curves when their flexural resonance frequency is tracked as a function of temperature. Such frequency shifts can be successfully used to monitor structural variations in DNA complexes, such as B-to-A form and helix-to-coil transitions, thus opening implications in both environmental studies—for example, trucking the effects of heavy metal exposure on human or vegetable DNA molecules—and in vitro experiments for the evaluation of the effects of drugs on patient DNA.

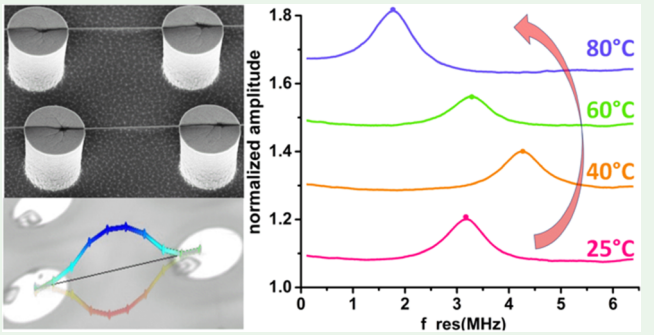

KEYWORDS: *DNA−ligand complexes, DNA structure, structural transitions, mechanical nanoresonator, nano-biosensing*

INTRODUCTION

The peculiar double-helix architecture gives DNA unique mechanical properties in terms of structural flexibility and enhanced stiffness, which are of fundamental importance in many biological processes. For example, a structural helix-to-coil transition is an unstacking event of the base pairs, with the breaking of H-bonds, typically involved in transcription and replication. Another example concerns the transitions from B to A form with peculiar bending and twisting properties, such as supercoiling, necessary for DNA packaging in cells and interaction with proteins.[1] For these reasons, DNA mechanical properties have been widely investigated by biologists and physicists, both from a theoretical and experimental point of view.[2−6]

The advancement in nanofabrication and force evaluation techniques led to the establishment of DNA manipulation and force measurements as tools for DNA mechanical investigation. In techniques such as magnetic/optical tweezers,[7−11] optical traps, DNA rulers,[12] and atomic force microscopy (AFM) force spectroscopy,[13−16] one extremity of DNA molecules is immobilized onto a treated surface, while the other one is anchored to a metallic nanoparticle, bead, or AFM tip. By moving the anchoring object, the DNA molecule is stretched while the applied force is measured. Alternatively, AFM peak force measurements can be performed on DNA molecules adsorbed on a surface, to recover the extent of deformation as a function of the applied pressure.[17]

All of these techniques successfully provide important information on DNA conformation and elastic parameters, but show several limitations such as strong dependence on the substrate, on the necessity to chemically modify the DNA for surface anchoring, and on DNA perturbation when pulling from surface anchoring. Moreover, the usual DNA length is limited to oligonucleotides (max 200 base pairs), resulting in mechanical information that would be hardly valid for long genomic DNA involved in real biological processes.

A different strategy was followed by Domínguez et al. to acquire information about the mechanical properties of 2D-DNA film grafted on the surface of a gold-coated microcantilever resonator. The authors tracked simultaneously the static bending and the dynamic change of resonance frequency of the grafted microcantilever as a function of the room humidity, thus reconstructing the elastic parameter of the DNA film.[18,19]

In a previous study, our group evaluated the mechanical properties of DNA complexes by a novel approach based on the measurement of the resonance frequency of suspended

Received: December 31, 2022
Accepted: January 18, 2023
Published: January 27, 2023

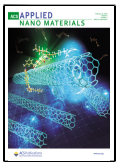

https://doi.org/10.1021/acsanm.2c05601
ACS Appl. Nano Mater. 2023, 6, 2249−2257

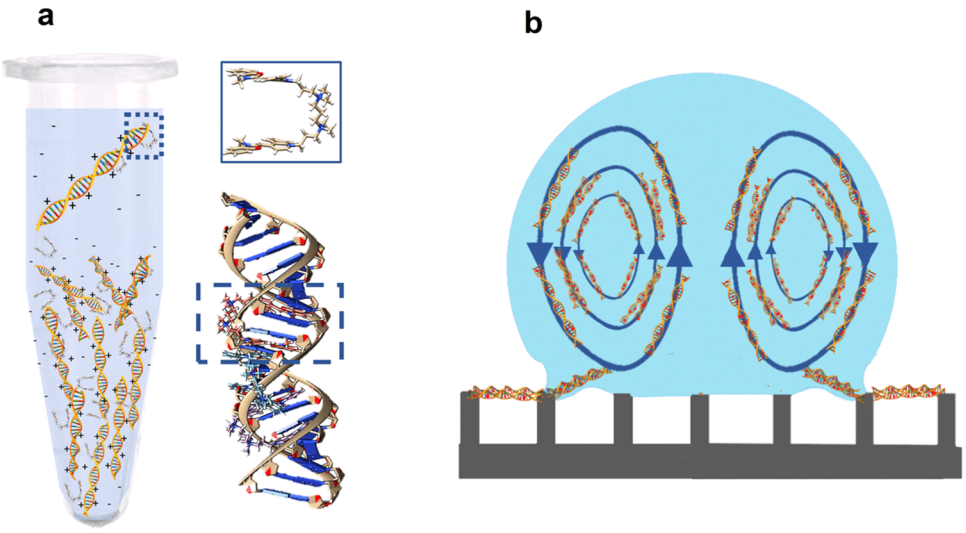

Figure 1. (a) Schematic representation of the DNA-YOYO-1 incubation. The solution containing λDNA and YOYO-1 molecules (whose fork shape is shown in the upper box) is kept for 2 h in physiological solution at 37 °C; the counterions, shielding the negative DNA backbones are represented by means of the symbols "+". At the end of the process, the DNA is intercalated, with a YOYO-molecule each with four bases (intercalation highlighted in the dotted box on the magnified scheme of the DNA intercalated molecule). (b) Scheme of the evaporation process: the red points on the DNA molecules represent the interacted ligand since when the droplet is placed on the SHS, all of the chemical interactions already took place during the previous incubation.

DNA nanobundles.[20] With a well-established method,[21−23] DNA complexes were suspended between superhydrophobic silicon micropillars acting as double-clamped nanomechanical resonators. Remarkably, the flexural behavior of these structures can be directly correlated to the elastic parameters of the corresponding DNA complexes composing the bundles, as verified by comparing the experimental results to the simulated behavior of single double-helices. In this framework, vibrometrical analysis overcomes the limitations of the traditional single-molecules technique, since it is real time, contactless, and no functionalization of DNA molecules is needed, thus widening the possible range of applications to genomic nucleic acids.

In this work, we show that DNA nanomechanical resonators can be successfully used for the real-time investigation of structural transitions in DNA complexes, by tracking their flexural resonance frequency as a function of temperature. Pristine double-stranded DNA (dsDNA), dsDNA bisintercalated with YOYO-1 or cisplatin, and single-stranded DNA (ssDNA) were monitored and compared, revealing that each DNA complex shows a unique fingerprint curve that can be linked to its proper structural transitions. Furthermore, in the case of pristine dsDNA, a sigmoidal melting curve can be derived from vibrational characteristics, and the corresponding melting temperature can be estimated.

Further studies could make this tool a valid alternative to high-resolution melting analysis for the investigation of DNA epigenetic features, such as methylation, or point mutations involved in carcinogenesis or genetic diseases. Furthermore, new implications will concern both environmental studies—for example, trucking the effects of heavy metal exposure on human or vegetable DNA molecules—and in vitro experiments for the evaluation of the effects of new drugs on patient DNA.

EXPERIMENTAL METHODS

Suspended DNA nanoresonators were prepared by starting from four different DNA solutions: double-stranded λ-DNA (48 502 bp sequence, New England Biolabs (NEB), Ipswich, Massachusetts), λ-dsDNA interacted with CisPt (Alfa Aesar, Karlsruhe, Germany, MW: 300 g/mol), λ-dsDNA bisintercalated with YOYO-1 (Thermo Fisher, Waltham, Massachusetts; MW: 1.271 g/mol), and single-stranded DNA of calf thymus (Sigma-Aldrich, St. Louis, Missouri).

For all of the samples, the DNA precursor was diluted in buffer solution (PBS 1×) at a final concentration of 50 ng/μL, and it was preheated at 65 °C for 10 min, to avoid any unwanted hybridization event between partially complementary sequences. After 30 min of incubation at 37 °C, 5 μL drops were deposited on the top of a superhydrophobic substrate (SHS), prepared as previously reported by Marini et al.,[24] while in the case of DNA interacalated with a saturating amount of YOYO-1 or CisPt, an additional incubation at 37 °C for 2 h is needed.

In any case, after the drop is positioned on the SHS, the solvent evaporation in a controlled environment (21 °C and ∼50% RH) leads to an uneven heat distribution inside the droplet, which provokes circular convective flows.[25,26] Thanks to this phenomenon, the molecules in solution are constantly mixed, and during the droplet volume reduction, the DNA strands are pulled between one pillar and the proximal one.[27] Schematic representations of the incubation process in the case of YOYO-1 intercalant and of the evaporation and suspension process are reported in Figure 1a,b, respectively.

The obtained suspended bundles were imaged by scanning electron microscopy (Fesem Supra 40, Zeiss, Oberkochen, Germany) with a working distance equal to 2.5 mm, acceleration voltage of 5 keV, and aperture size of 30 μm; no metal coating was applied to the samples (see Figure S1). The length and diameter of each bundle were evaluated, respectively, through ImageJ and Gatan Microscopy Suite Software, a free version from Ametek, as reported in Figure S2.

The vibrational analysis of the DNA resonators was performed through a laser Doppler vibrometer (MSA-500, Polytec Gmbh, Waldbronn, Germany), with nominal displacement and velocity resolution, respectively, <0.4 pm/$\sqrt{\text{Hz}}$ and <1 μm/s. The laser (633 nm) was focused roughly in the middle of the bundles by means of a 100× objective lens (PLAN Apochromat, 0.55 N.A., 13 mm WD, Motic., Hong Kong) used also to collect the reflected light, whose frequency is different from the incident one due to the Doppler effect. Its interference with the reference beam gives the amplitude and frequency of vibration of the resonating structure. The laser spot focused on the bundle is approximately 1 μm wide, such that the highest reflectivity of the laser is approximately 60%.

https://doi.org/10.1021/acsanm.2c05601
ACS Appl. Nano Mater. 2023, 6, 2249−2257

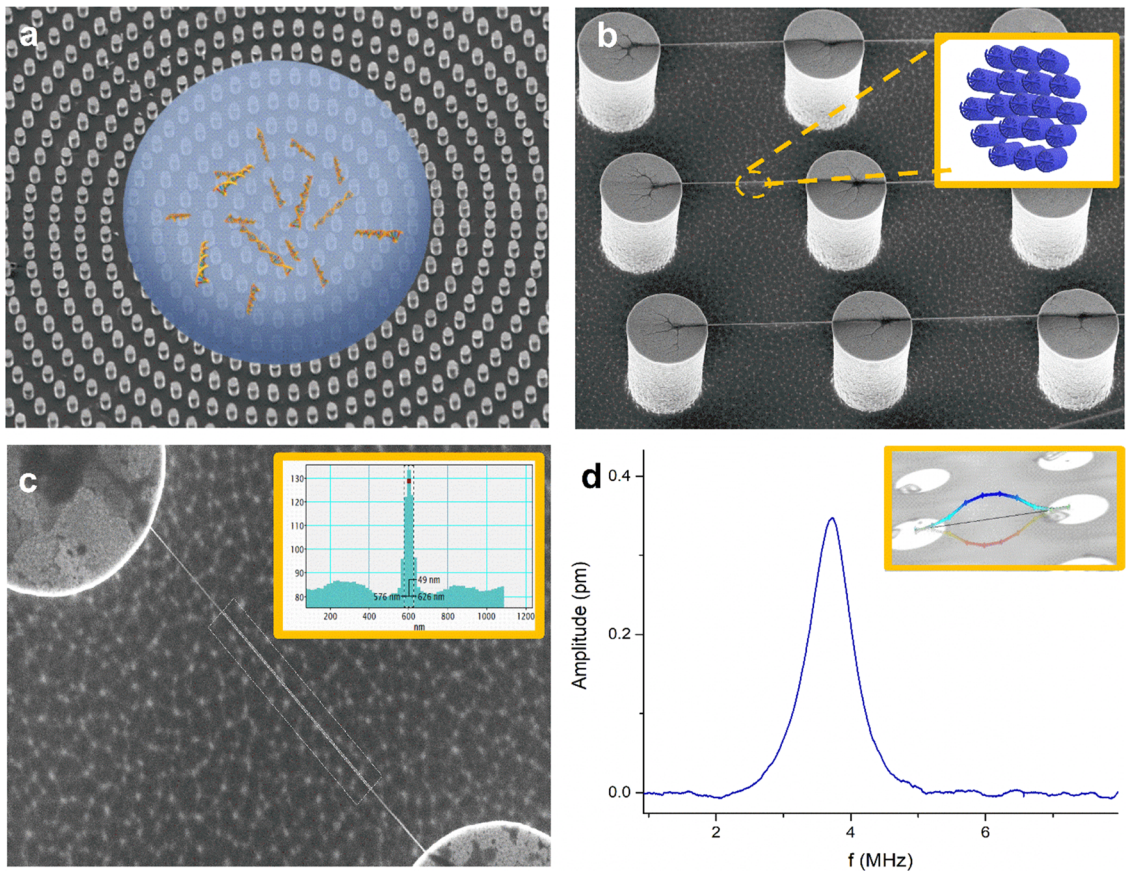

Figure 2. Scanning electron microscopy (SEM) pictures of (a) the SHS with a scheme of the evaporation process; the circular pattern of the pillars guides the evaporation direction and leads to the formation of the DNA bundles; (b) DNA bundles suspended between silicon micropillars; the inset shows the scheme of the geometrical organization of the strands inside the bundles; and (c) a single suspended bundle, with its diameter (49 nm) evaluated by Gatan software in the inset. (d) Vibrational spectrum of one dsDNA nanoresonator; the inset shows the reconstruction of the vibrational amplitude, obtained using a laser Doppler vibrometer.

The measurements were performed in air, with no actuation; the thermomechanical vibration spectrum was obtained with 500 averages, to maximize the signal-to-noise ratio, with a bandwidth of 10 MHz and a spectral resolution of approximately 48 Hz. The samples were mounted on a Peltier cell to perform the temperature ramp. The temperature was changed each 5 °C between 25 and 80 °C. The vibrational spectra were measured 10 min after the temperature was set to avoid temperature gradients in the samples.

RESULTS AND DISCUSSION

DNA nanomechanical resonators were fabricated by a straightforward approach based on superhydrophobic substrates (SHSs) with several concentric silicon pillars (diameter of 6 μm, uniform all over the wafer). This geometrical pattern guides the direction of evaporation of a drop of solution containing the desired DNA molecules, which are pulled between one pillar and the proximal one during the process (Figure 2a). Such a technique allows the formation of a large number of suspended DNA bundles on a single chip (Figure 2b), preferentially aligned in the radial direction; they have different diameters depending on the distance from the center of the chip, where the droplet evaporation residue is localized (Figure S1). These bundles are composed of DNA strands following a geometrical pattern and organized in shields (scheme in the inset of Figure 2b), each one surrounded by water molecules, as previously shown by transmission electron microscopy (TEM) analysis.[28] For this study, we analyzed bundles with diameters in the range of 40−100 nm (Figure 2c) and lengths between 6 and 14 μm. The variability in length is ascribed to the different orientations of the bundle with respect to the radial direction and to the final bundle anchoring points on the pillar, as it is possible to appreciate in Figure S3. The resonance frequency of DNA double-clamped resonators depends on their geometry and their elastic parameter according to eq 1

$$f_n = \frac{\lambda_n^2}{4\pi L^2}\sqrt{\frac{ER^2}{\rho}} \quad (1)$$

where L, R, E, and ρ are, respectively, the length, the radius, Young's modulus, and the density of the bundles, while λ_n is the modal factor (4.73 for the first resonance frequency). It follows that for bundles with different sizes, different natural resonance frequencies are expected.

A typical vibrational spectrum for a DNA nanoresonator obtained in air at room temperature is shown in Figure 2d: the thermomechanical peak is clearly emerging from the background noise, and the corresponding first flexural mode is reconstructed in the inset, by measuring the out-of-plane displacement in 10 different points along the dsDNA bundle. The quality factor of these structures, computed as the ratio between the resonance frequency and the bandwidth at −3 dB, is in the order of few units (from 3 to 7), in agreement with previous experiments.[20]

https://doi.org/10.1021/acsanm.2c05601
ACS Appl. Nano Mater. 2023, 6, 2249−2257

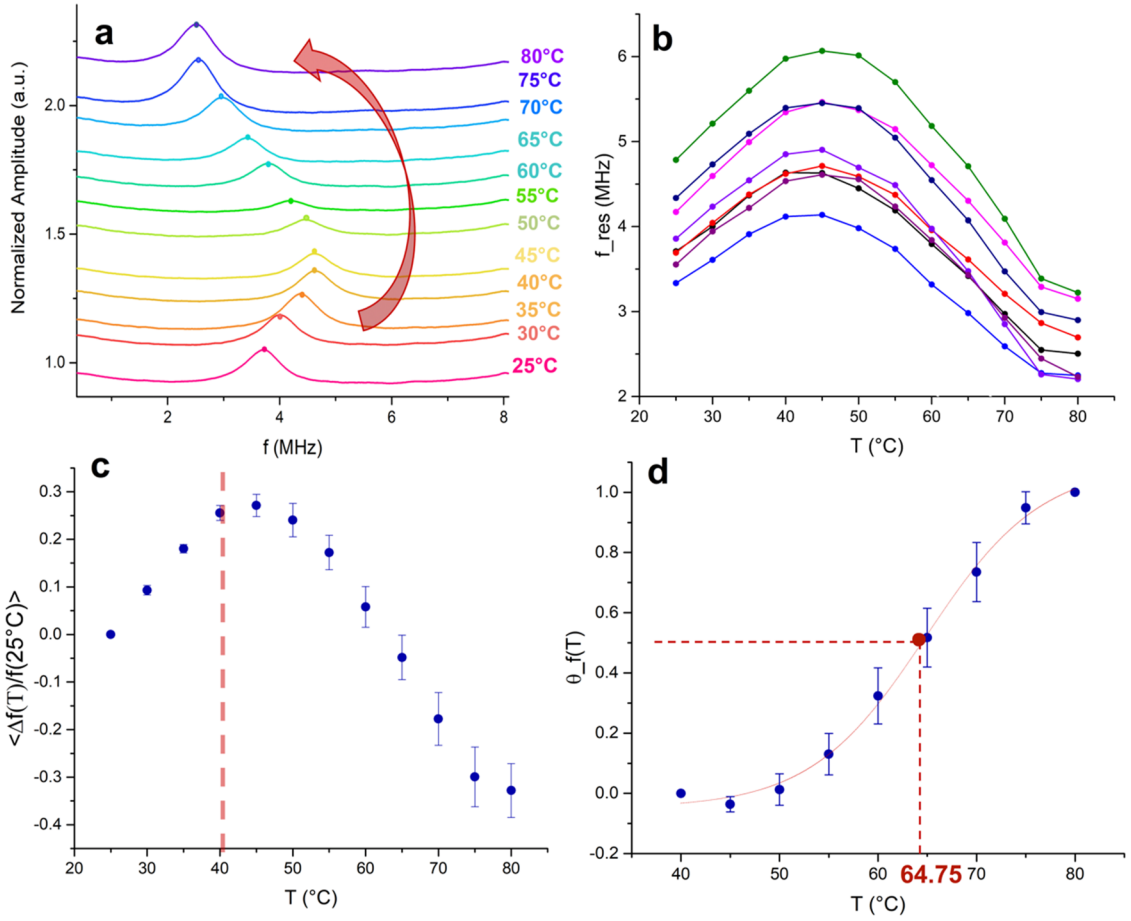

Figure 3. (a) Normalized vibrational spectra of a dsDNA nanoresonator at different temperatures (the curves were translated in the *y*-axis for a clearer comparison); (b) evolution of the resonance frequency as a function of temperature for eight dsDNA nanoresonators; (c) average relative frequency deviation for bundles of the central family in panel (b); and (d) melting curve of the analyzed dsDNA nanoresonators.

The repeatability of these measurements was assessed by acquiring the resonance frequency of several suspended bundles, under fixed air conditions (constant T and RH), once each 5 min for 12 times (~1 h). The results are reported in Table S1 and show a relative uncertainty of the resonance frequency lower than 0.5% for all of the samples. This variability increased to an average value of 1.6% repeating the measurements after 3−5 h, which coincides with the typical time scale of the experiments performed in this work. It follows that, given stable environmental conditions, the resonance frequency of the DNA nanoresonators can be considered repeatable, within a relative experimental uncertainty lower than 2%.

Temperature Dependence of dsDNA Nanoresonators. DNA mechanical properties are strongly dependent on the temperature of the strands; thus, the resonance frequency of our resonators varies accordingly. The vibrational spectra measured at different temperatures (from 25 to 80 °C) for a dsDNA nanoresonator are reported in Figure 3a, where a nonmonotonic shift of the resonance frequency according to the set temperature is clearly visible. The evolution of the resonance frequencies of eight suspended bundles of dsDNA, as a function of the temperature, can be appreciated in Figure 3b. The natural resonance frequency at 25 °C shows a variability of 12%; it was evaluated as the standard deviation of the eight bundles and can be ascribed to the slightly different sizes of the resonators, as reported in Table S2. Despite that, a clear fingerprint can be recognized in the frequency evolution for all eight bundles, since all of them follow the same relative variation trend.

The behavior of the bundles can be more efficiently tracked by removing their geometrical dependence with the frequency deviation $f'(T)$ calculated for each bundle as

$$f'(T) = \frac{\Delta f(T)}{f(25^\circ\mathrm{C})} = \frac{f(T) - f(25^\circ\mathrm{C})}{f(25^\circ\mathrm{C})} = \sqrt{\frac{E(T)}{E(25^\circ\mathrm{C})}}\sqrt{\frac{\rho(25^\circ\mathrm{C})}{\rho(T)}} - 1 \quad (2)$$

Assuming that the geometry is constant during the process, R and L of each bundle simplify through the normalization with $f(25\ ^\circ\mathrm{C})$ and f' is independent of them. In Figure 3c, the average evolution of this new figure of merit is reported. Error bars are taken as the standard deviation between the eight examined bundles; it significantly increases with the temperature, as a consequence of thermal noise. Despite that, the highest value of the relative standard deviation at 75 °C is less than 10%, thus confirming that all of the dsDNA nanoresonators act in good agreement and that the frequency variation at each temperature is well separated from the previous one.

From 25 to 40 °C, the average frequency deviation increases almost linearly with the temperature. As a first analysis, this effect could be attributed to the mass loss by the suspended

https://doi.org/10.1021/acsanm.2c05601
ACS Appl. Nano Mater. 2023, 6, 2249−2257

bundles through water desorption. In fact, the mechanical resonators can be treated as one-dimensional (1D) harmonic oscillators, whose resonance frequency is equal to

$$f = \frac{1}{2\pi}\sqrt{\frac{k}{m}} \tag{3}$$

where k and m are, respectively, the spring constant and the mass of the resonator. In the field of biosensing, the following relationship can be deduced and widely used to track the change in resonance frequency (Δf) due to the mass adsorbed (Δm) onto the surface of inorganic micro/nanoresonators: $\frac{\Delta f}{f_0} = -\frac{1}{2}\frac{\Delta m}{m_0}$.

However, such a relation is only valid if the added mass is much smaller than the initial resonator mass and if the resonator density and spring constant remain unchanged. In our reported experiments, these two conditions may not be verified since the water loss is distributed along the entire length of the bundles, penetrating the inner shells. In fact, the average normalized resonance frequency at 40 °C is approximately 25% higher than the initial one at 25 °C and this variation would require the evaporation of more water than the one present at the beginning in the bundles, according to the previously explained shell model. It follows that in the first part of the curve, together with water desorption, structural reinforcement of the suspended bundles is expected, which can be attributed to the conformational transition of the inner dsDNA molecules from B to A form. These are two of the most widespread DNA conformations in nature, and they differ for several structural parameters, such as the base pairs per turn (bp/turn) and the rise/turn which are, respectively, 11 and 0.25 nm in the A-form and of 10 and 0.34 nm in the other case. It follows that A-DNA is more compact than B-DNA; moreover, it presents a larger helix diameter (2.3 nm instead of 2 nm) since the base pairs are displaced from the helix axis,[29] which makes it stiffer with respect to the B-form (Figure S4). Such forms can interchange according to the DNA sequence, DNA functions (replication, DNA−protein interaction), and environmental conditions: the A-form, in fact, is the preferred conformation for humidity lower than 75%.[30] In this work, all of the measurements were performed in air (RH ∼ 50%). Under these conditions, or in vacuum, the outer shells of the bundles have to be in the dehydrated A-form, as observed by Marini et al. through high-resolution transmission microscopy (HRTEM), which showed a structure of the helix at the edge of the DNA bundle perfectly compatible with the geometrical sizes of the A-form.[24] dsDNA bundles were also analyzed through nondestructive Raman spectroscopy, which revealed the presence of both A-form and B-form in the same bundles.[31] The B-form contribution is related to helices inside the bundles, which retained water molecules, rather than the external dehydrated helices shells. We can thus argue that the heating up of the samples causes a partial evaporation of the water stored inside the bundles, allowing the previously hydrated DNA molecules to transit from B-form to A-form. This transition may increase the effective spring constant of the resonator, since the A-form is stiffer than the B-form, thus explaining the relatively large increment of resonance frequency in the first part of the plot in Figure 3c. Another possible effect of the heating process could be the loss or segregation of counterions together with the water desorption, which could cause electrostatic repulsion between the strands, changing the mechanical response of the resonators. Other effects that would soften the structure—thus decreasing the frequency, such as premelting—could be present, but with a minor impact.

For temperatures higher than 40 °C, while the water desorption reasonably continues with a lower rate, a new effect clearly rises, being then the dominant one in the range of 50−80 °C, where the resonance frequency shows an almost linear decrease with the applied temperature. Such an effect needs to be associated with a progressive softening of the structure since, as previously commented, the water desorption and the transition from B to A form would continue to stiffen the structure, thus increasing the resonance frequency, instead of decreasing it. Thus, such a decrease in resonance frequency can be straightforwardly ascribed to the signature of DNA denaturation, i.e., of the helix−coil transition. During this process, the energy provided to the molecules by heating is used to break the hydrogen bonds between the bases and thus to open the complementary strands of the double helices. Denaturation changes several DNA properties, including viscosity and optical activity, leading for example to hyperchromicity. In fact, one of the most reliable indicators of amine base unstacking is the increase in UV absorbance,[32] which is efficiently used to reconstruct a typical melting curve. The fraction of denatured base pairs $\Theta_A(T)$ can be written as a function of the normalized absorbance A, at each T and at the initial and final ones (T_0, T_{fin})

$$\Theta_A(T) = \frac{A(T) - A(T_0)}{A(T_{fin}) - A(T_0)} \tag{4}$$

This relation is commonly used to reconstruct the melting curve of DNA in solution. In Figure 3d, it is possible to appreciate the melting curve related to the DNA nanoresonators analyzed in this work, found by substituting in eq 4 the absorbance with the average resonance frequency deviation

$$\Theta_f(T) = \frac{\langle f'(T)\rangle - \langle f'(T_{in})\rangle}{\langle f'(T_{fin})\rangle - \langle f'(T_{in})\rangle} \tag{5}$$

where T_{in} and T_{fin} are, respectively, 40 and 80 °C, when the melting process begins and ends. The melting curve follows a clear sigmoidal function (R^2 of the fit equal to 0.99), typical of the helix-to-coil cooperative transition, in which denaturation bubbles initially appear in AT-rich regions and then gradually grow in size and number with temperature.[33,34] The number of base pairs of the λDNA molecules (∼50k) allows obtaining multiple denaturation sites, which propagate until the complete denaturation of the double helix. As commonly reported in the literature, the melting temperature is for convention chosen as the temperature for which $\Theta = 0.5$.[35] The obtained value for our suspended DNA bundles of roughly 50k bp is 64.75 °C, i.e., lower than 94 °C, the value expected for the same DNA sequence through traditional methods.[36] Such a decrement is expected since low-dimensional nanostructures generally tend to have a lower melting point with respect to their related bulks because of their drastically higher surface-to-volume ratio. Furthermore, in traditional techniques, the DNA molecules are in physiological buffer, where the ions in solution dynamically shield the repulsive force between the phosphate groups of DNA backbones, thus stabilizing the structure and delaying the denaturation starting point. On the contrary, the DNA molecules of the presented nanoresonators are in an air environment; moreover, the evaporation process produces a self-sieving effect such that the helices retain only

https://doi.org/10.1021/acsanm.2c05601
ACS Appl. Nano Mater. 2023, 6, 2249−2257

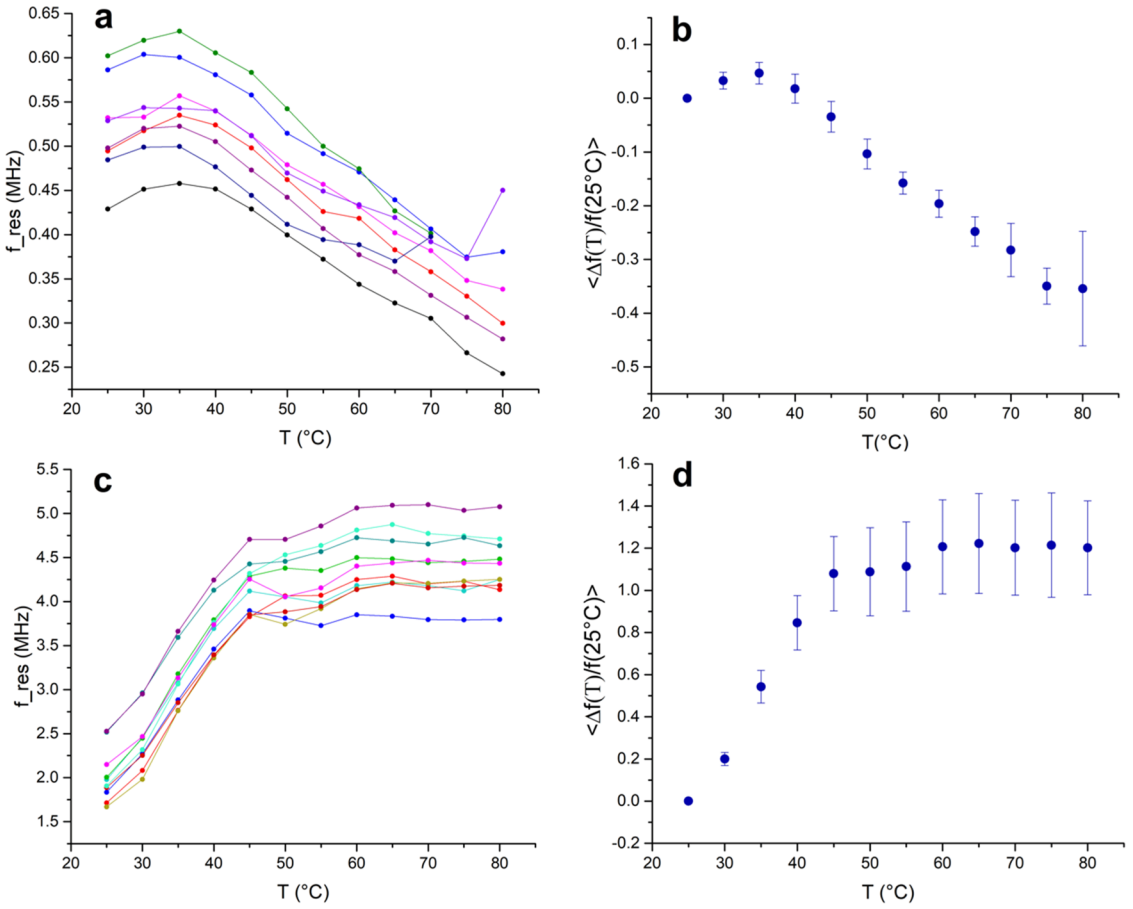

Figure 4. (a) Evolution of the resonance frequency as a function of temperature for dsDNA + CisPt nanoresonators; (b) average relative frequency deviation for the bundles in panel (a); (c) evolution of the resonance frequency as a function of temperature for 10 dsDNA + YOYO-1 nanoresonators; and (d) average relative frequency deviation for the ten bundles in panel (c).

the ions that effectively have interacted with the DNA strand in solution.[37]

It is worth emphasizing once again that each analyzed DNA nanoresonator is composed of several DNA molecules organized and constrained in bundles. In this framework, the melting curve of the DNA nanoresonator obtained through a noncontact real-time vibrometrical analysis is a particularly remarkable result since it strengthens the role of this technique as a valid candidate toward real-time single-molecule structural analysis.

Furthermore, in the Supporting Information (Figure S5), it is possible to observe also the results of the experiments conducted on a different day on the same set of samples. The air humidity was 9% lower than that during the first set of measurements, and the resonance frequency of the bundles was an average 10% higher than that in the previous results. Such an increment in the frequency is coherent with both an associated decrease of water mass, according to eq 3, and a larger fraction of DNA bundles in the dehydrated A-form, i.e, the stiffer one. Despite this relatively large variability, the fingerprint in temperature was clearly the same, thus providing further proof that the information observed by this method is structural and is not affected by the initial conditions of the resonators; moreover, they demonstrate the reproducibility of the measurements, which let us assess that both the transitions observed above are reversible.

Similar measurements were also performed on bundles with different lengths: $L = 14.10 \pm 0.12$ μm and $L = 7.11 \pm 0.34$ μm. The results are shown in Figure S6: despite the different initial resonance frequencies, the fingerprint of the curve in temperature is the same, proving that the observed transitions are independent of the geometry (i.e., on the initial mass and frequency of the resonators) and must be linked to structural transitions of the molecules composing the bundles.

Temperature Dependence of Different DNA Nanoresonators. The same analysis was performed on mechanical nanoresonators composed of dsDNA intercalated with the chemotherapeutic agent CisPlatin (CisPt). CisPt is an inorganic compound with a platinum agent that covalently bonds with N7 of purine bases, causing severe alteration of the DNA double helix, as well as disruption of the base pair H-bonds.[38] As reported in Figure 4a,b, a similar fingerprint is shown when resonance frequencies of individual bundles (Figure 4a) and their average relative frequency deviation (Figure 4b) are plotted versus temperature: first a monotonic increase (attributed to water desorption and structural transition from B to A form) and then a progressive decrease due to DNA denaturation. Since parts of the base pairs are already disrupted here by the CisPt ligand at saturation, clear differences with respect to pristine dsDNA are expected for the absolute temperatures of transitions. The helix-to-coil transition starts to affect the resonance frequency at a temperature 15 °C lower than that of the pristine dsDNA case, while the melting temperature is lowered to 57 °C. These results highlight the possible use of these analyses to investigate the

https://doi.org/10.1021/acsanm.2c05601
ACS Appl. Nano Mater. 2023, 6, 2249−2257

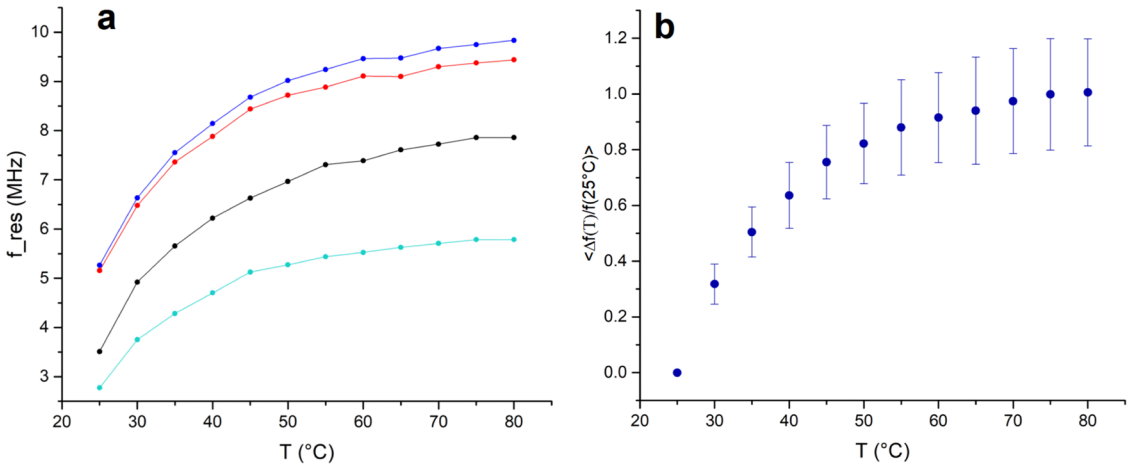

Figure 5. (a) Evolution of the resonance frequency as a function of temperature for ssDNA nanoresonators used as the negative control; and (b) average relative frequency deviation for the bundles in panel (a).

mechanical alterations induced in DNA by drugs such as chemotherapeutic agents.

A third case of study is dsDNA intercalated with YOYO-1 molecules. YOYO-1 is a bisintercalator with a fork shape (Figure S2), which places itself between two base pairs each four. The intercalation with YOYO-1 molecules affects the pristine dsDNA molecule, increasing its turn length and stiffness.[20] In Figure 4c, the evolution of the resonance frequency of 10 DNA + YOYO-1 nanoresonators as a function of temperature is reported, and the corresponding average frequency deviation is shown in Figure 4d. As in the previous cases, all of the resonance frequencies show a similar monotonic increase with temperatures lower than 40° for which the same considerations about water desorption and structural transition from B to A form can be done. However, starting from 40 °C, we do not observe a maximum or the well-definite signature of denaturation as in previous cases since the curve reaches a plateau region. It can be concluded that the presence of YOYO-1 stabilizes the mechanical properties and thus the resonance frequency of the dsDNA nanoresonators: the bisintercalant acts as a clamp and keeps in place the DNA hemihelices, thus preventing the total opening of the DNA molecules and thus the progressive softening of the whole structure.

To conclude the analysis, the same measurements were performed on ssDNA bundles with different lengths, reported in Table S3, which can be effectively used as a negative control, since such DNA molecules cannot undergo helix-to-coil structural transitions. This hypothesis is verified by the absence of a drop in the frequency or of a plateau region above 40 °C (Figure 5a,b, where resonance frequencies of individual bundles and their average relative frequency deviation are plotted, respectively). On the other hand, the smooth monotonic increase of the resonance frequency can be ascribed to the base unstacking given by the thermal energy provided to the system,[39] which adds rotational and torsional degrees of freedom to the nucleotides of the ssDNA molecules.

CONCLUSIONS

In this work, we established a new, contactless, and label-free method for the real-time monitoring of DNA temperature-dependent structural transitions, through the vibrometrical analysis of mechanical nanoresonators made of different DNA complexes. In the case of pristine dsDNA bundles, we can clearly recognize a fingerprint in the resonance frequency evolution that can be ascribed to the helix-to-coil transition. In fact, even if the loss of water and counterions reasonably continues after 40 °C, their contribution tends to increase the stiffness of the structure, contrarily to the dsDNA denaturation, which softens the bundles. Given the measured decrease in resonance frequency, their effect above 40 °C has to be of minor importance. We have also defined the melting temperature of the dsDNA composing the bundles, opening a way for the future use of this tool to investigate DNA epigenetic features, such as, for example, methylation, which strongly influence the DNA melting point and correlate to several diseases. Moreover, different intercalating agents induced clear alterations in the fingerprint curve, thus revealing their specific structural role during the temperature-depended structural transitions studied here.

The SHS-DNA system proposed here autonomously concentrates the DNA molecules in a small and well-defined region of the sample down to the attomolar level, overcoming the limit of the need for an amplification process. Furthermore, it is label-free, and it is tailored to evaluate and study long DNA strands, such as nucleic acids extracted from cells: analyzing the 50k bp long λDNA represents an important step toward genomic DNA analysis. On the contrary, cutting-edge fluorescence-based techniques, such as high-resolution melting analysis, show high sensitivity and reliability of the results, but face intrinsic limitations: they require the amplification of the sequence of interest, which is typically limited to few hundreds of bp long, and the intercalation of DNA with a fluorescent dye.

We, therefore, envision that this method could have important implications in both environmental studies—for example, trucking the effects of heavy metal exposure on human or vegetable DNA molecules—and in vitro experiments for the evaluation of the effects of new drugs on patient DNA.

ASSOCIATED CONTENT

Supporting Information

The Supporting Information is available free of charge at https://pubs.acs.org/doi/10.1021/acsanm.2c05601.

Additional experimental results: SEM images of the result of the suspension process, geometrical dimension

https://doi.org/10.1021/acsanm.2c05601
ACS Appl. Nano Mater. 2023, 6, 2249−2257

of the analyzed samples, and temperature dependence of the sample on a different day; graphical representation of the different DNA molecules composing the bundles (PDF)

AUTHOR INFORMATION

Corresponding Author

Carlo Ricciardi − *Department of Applied Science and Technologies (DISAT), Politecnico di Torino, 10129 Torino, Italy;* orcid.org/0000-0002-4703-7949; Email: carlo.ricciardi@polito.it

Authors

Francesca Legittimo − *Department of Applied Science and Technologies (DISAT), Politecnico di Torino, 10129 Torino, Italy;* orcid.org/0000-0002-2912-6868

Monica Marini − *Department of Applied Science and Technologies (DISAT), Politecnico di Torino, 10129 Torino, Italy;* orcid.org/0000-0001-8182-5239

Stefano Stassi − *Department of Applied Science and Technologies (DISAT), Politecnico di Torino, 10129 Torino, Italy;* orcid.org/0000-0002-1134-7224

Enzo Di Fabrizio − *Department of Applied Science and Technologies (DISAT), Politecnico di Torino, 10129 Torino, Italy;* orcid.org/0000-0001-5886-4678

Complete contact information is available at: https://pubs.acs.org/10.1021/acsanm.2c05601

Author Contributions

S.S. and C.R. conceived the experiment. M.M. and F.L. prepared the samples. F.L. performed the measurements and analyzed the nanomechanical data with S.S. and C.R. M.M. and E.D.F. proposed the biomolecular interpretations. F.L. wrote the draft and all authors contributed to finalizing the manuscript.

Notes

The authors declare no competing financial interest.

REFERENCES

(1) Basu, A.; Bobrovnikov, D. G.; Ha, T. DNA Mechanics and Its Biological Impact. *J. Mol. Biol.* **2021**, *433*, No. 166861.

(2) Garai, A.; Saurabh, S.; Lansac, Y.; Maiti, P. K. DNA Elasticity from Short DNA to Nucleosomal DNA. *J. Phys. Chem. B* **2015**, *119*, 11146−11156.

(3) Bustamante, C.; Bryant, Z.; Smith, S. B. Ten Years of Tension: Single-Molecule DNA Mechanics. *Nature* **2003**, *421*, 423−427.

(4) Garcia, H. G.; Grayson, P.; Han, L.; Inamdar, M.; Kondev, J.; Nelson, P. C.; Phillips, R.; Widom, J.; Wiggins, P. A. Biological Consequences of Tightly Bent DNA: The Other Life of a Macromolecular Celebrity. *Biopolymers* **2007**, *85*, 115−130.

(5) Savelyev, A.; Materese, C. K.; Papoian, G. A. Is DNA' s Rigidity Dominated by Electrostatic or Nonelectrostatic. *J. Am. Chem. Soc.* **2011**, *133*, 19290−19293.

(6) Mantelli, S.; Muller, P.; Harlepp, S.; Maaloum, M. Conformational Analysis and Estimation of the Persistence Length of DNA Using Atomic Force Microscopy in Solution. *Soft Matter* **2011**, *7*, 3412−3416.

(7) Schöpflin, R.; Brutzer, H.; Müller, O.; Seidel, R.; Wedemann, G. Probing the Elasticity of DNA on Short Length Scales by Modeling Supercoiling under Tension. *Biophys. J.* **2012**, *103*, 323−330.

(8) Celedon, A.; Nodelman, I. M.; Wildt, B.; Dewan, R.; Searson, P.; Wirtz, D.; Bowman, G. D.; Sun, S. X. Magnetic Tweezers Measurement of Single Molecule Torque. *Nano Lett.* **2009**, *9*, 1720−1725.

(9) Xin, Q.; Li, P.; He, Y.; Shi, C.; Qiao, Y.; Bian, X.; Su, J.; Qiao, R.; Zhou, X.; Zhong, J. Magnetic Tweezers for the Mechanical Research of DNA at the Single Molecule Level. *Anal. Methods* **2017**, *9*, 5720−5730.

(10) Bustamante, C.; Smith, S. B.; Liphardt, J.; Smith, D. Single-Molecule Studies of DNA Mechanics. *Curr. Opin. Struct. Biol.* **2000**, *10*, 279−285.

(11) Strick, T.; Allemand, J. F.; Croquette, V.; Bensimon, D. Twisting and Stretching Single DNA Molecules. *Prog. Biophys. Mol. Biol.* **2000**, *74*, 115−140.

(12) Chen, T.; Hong, Y.; Reinhard, B. M. Probing DNA Stiffness through Optical Fluctuation Analysis of Plasmon Rulers. *Nano Lett.* **2015**, *15*, 5349−5357.

(13) Camunas-Soler, J.; Ribezzi-Crivellari, M.; Ritort, F. Elastic Properties of Nucleic Acids by Single-Molecule Force Spectroscopy. *Annu. Rev. Biophys.* **2016**, *45*, 65−84.

(14) Main, K. H. S.; Provan, J. I.; Haynes, P. J.; Wells, G.; Hartley, J. A.; Pyne, A. L. B. Atomic Force Microscopy—A Tool for Structural and Translational DNA Research. *APL Bioeng.* **2021**, *5*, No. 031504.

(15) Chaurasiya, K. R.; Paramanathan, T.; McCauley, M. J.; Williams, M. C. Biophysical Characterization of DNA Binding from Single Molecule Force Measurements. *Phys. Life Rev.* **2010**, *7*, 299−341.

(16) Williams, M. C.; Rouzina, I. Force Spectroscopy of Single DNA and RNA Molecules. *Curr. Opin. Struct. Biol.* **2002**, *12*, 330−336.

(17) Li, L.; Zhang, P.; Li, J.; Wang, Y.; Wei, Y.; Hu, J.; Zhou, X.; Xu, B.; Li, B. Measurement of Nanomechanical Properties of DNA Molecules by PeakForce Atomic Force Microscopy Based on DNA Origami. *Nanoscale* **2019**, *11*, 4707−4711.

(18) Domínguez, C. M.; Ramos, D.; Mendieta-Moreno, J. I.; Fierro, J. L. G.; Mendieta, J.; Tamayo, J.; Calleja, M. Effect of Water-DNA Interactions on Elastic Properties of DNA Self-Assembled Monolayers. *Sci. Rep.* **2017**, *7*, No. 536.

(19) Domínguez, C. M.; Kosaka, P. M.; Mokry, G.; Pini, V.; Malvar, O.; Del Rey, M.; Ramos, D.; Paulo, A. S.; Tamayo, J.; Calleja, M. Hydration Induced Stress on DNA Monolayers Grafted on Microcantilevers. *Langmuir* **2014**, *30*, 10962−10969.

(20) Stassi, S.; Marini, M.; Allione, M.; Lopatin, S.; Marson, D.; Laurini, E.; Pricl, S.; Pirri, C. F.; Ricciardi, C.; Di Fabrizio, E. Nanomechanical DNA Resonators for Sensing and Structural Analysis of DNA-Ligand Complexes. *Nat. Commun.* **2019**, *10*, No. 1690.

(21) Marini, M.; Limongi, T.; Falqui, A.; Genovese, A.; Allione, M.; Moretti, M.; Lopatin, S.; Tirinato, L.; Das, G.; Torre, B.; Giugni, A.; Cesca, F.; Benfenati, F.; Di Fabrizio, E. Imaging and Structural Studies of DNA-Protein Complexes and Membrane Ion Channels. *Nanoscale* **2017**, *9*, 2768−2777.

(22) Miele, E.; Accardo, A.; Falqui, A.; Marini, M.; Giugni, A.; Leoncini, M.; De Angelis, F.; Krahne, R.; Fabrizio, E. Di. Writing and Functionalisation of Suspended DNA Nanowires on Superhydrophobic Pillar Arrays. *Small* **2015**, *11*, 134−140.

(23) De Angelis, F.; Gentile, F.; Mecarini, F.; Das, G.; Moretti, M.; Candeloro, P.; Coluccio, M. L.; Cojoc, G.; Accardo, A.; Liberale, C.; Zaccaria, R. P.; Perozziello, G.; Tirinato, L.; Toma, A.; Cuda, G.; Cingolani, R.; Di Fabrizio, E. Breaking the Diffusion Limit with Super-Hydrophobic Delivery of Molecules to Plasmonic Nanofocusing SERS Structures. *Nat. Photonics* **2011**, *5*, 682−687.

(24) Marini, M.; Falqui, A.; Moretti, M.; Limongi, T.; Allione, M.; Genovese, A.; Lopatin, S.; Tirinato, L.; Das, G.; Torre, B.; Giugni, A.; Gentile, F.; Candeloro, P.; Di Fabrizio, E. The Structure of DNA by Direct Imaging. *Sci. Adv.* **2015**, *1*, No. e1500734.

(25) Pan, Z.; Dash, S.; Weibel, J. A.; Garimella, S. V. Assessment of Water Droplet Evaporation Mechanisms on Hydrophobic and Superhydrophobic Substrates. *Langmuir* **2013**, *29*, 15831−15841.

(26) Ressine, A.; Finnskog, D.; Marko-Varga, G.; Laurell, T. Superhydrophobic Properties of Nanostructured-Microstructured Porous Silicon for Improved Surface-Based Bioanalysis. *Nanobiotechnology* **2008**, *4*, 18−27.

(27) Zhang, P.; Moretti, M.; Allione, M.; Tian, Y.; Ordonez-Loza, J.; Altamura, D.; Giannini, C.; Torre, B.; Das, G.; Li, E.; Thoroddsen, S.

T.; Sarathy, S. M.; Autiero, I.; Giugni, A.; Gentile, F.; Malara, N.; Marini, M.; Di Fabrizio, E. A Droplet Reactor on a Super-Hydrophobic Surface Allows Control and Characterization of Amyloid Fibril Growth. *Commun. Biol.* **2020**, *3*, No. 457.
(28) Gentile, F.; Moretti, M.; Limongi, T.; Falqui, A.; Bertoni, G.; Scarpellini, A.; Santoriello, S.; Maragliano, L.; Proietti Zaccaria, R.; Di Fabrizio, E. Direct Imaging of DNA Fibers: The Visage of Double Helix. *Nano Lett.* **2012**, *12*, 6453−6458.
(29) Vologodskiĭ, A. V.DNA Structures. In *Biophysics of DNA*; Cambridge University press, 2015; pp 1−22.
(30) Franklin, R. E.; Gosling, R. G. Molecular configuration in sodium thymonucleate. *Nature* **1953**, *171*, 740−741.
(31) Marini, M.; Allione, M.; Torre, B.; Moretti, M.; Limongi, T.; Tirinato, L.; Giugni, A.; Das, G.; di Fabrizio, E. Raman on Suspended DNA: Novel Super-Hydrophobic Approach for Structural Studies. *Microelectron. Eng.* **2017**, *175*, 38−42.
(32) Hammouda, B.; Worcester, D. The Denaturation Transition of DNA in Mixed Solvents. *Biophys. J.* **2006**, *91*, 2237−2242.
(33) Zeng, Y.; Montrichok, A.; Zocchi, G. Bubble Nucleation and Cooperativity in DNA Melting. *J. Mol. Biol.* **2004**, *339*, 67−75.
(34) Blake, R. D. Cooperative Lengths of DNA during Melting. *Biopolymers* **1987**, *26*, 1063−1074.
(35) Nelson, D. L.; Cox, M. M.Nucleotidi e Acidi Nucleici. In *I Principi Di Biochimica Di Lehninger*, 7th ed.; Zanichelli, 2010; pp 291−322.
(36) Ivask, A.; Voelcker, N. H.; Seabrook, S. A.; Hor, M.; Kirby, J. K.; Fenech, M.; Davis, T. P.; Ke, P. C. DNA Melting and Genotoxicity Induced by Silver Nanoparticles and Graphene. *Chem. Res. Toxicol.* **2015**, *28*, 1023−1035.
(37) Marini, M.; Torre, B.; Allione, M.; Limongi, T.; Legittimo, F.; Giugni, A.; Ricciardi, C.; Pirri, C. F.; Fabrizio, E. Self-Sieving DNA over Superhydrophobic Surfaces: A Raman Spectroscopy Study. *J. Raman Spectrosc.* **2022**, *53*, 1352−1360.
(38) Eastman, A. The Formation, Isolation and Characterization of DNA Adducts Produced by Anticancer Platinum Complexes. *Pharmacol. Ther.* **1987**, *34*, 155−166.
(39) Zhou, J.; Gregurick, S. K.; Krueger, S.; Schwarz, F. P. Conformational Changes in Single-Strand DNA as a Function of Temperature by SANS. *Biophys. J.* **2006**, *90*, 544−551.

https://doi.org/10.1021/acsanm.2c05601
ACS Appl. Nano Mater. 2023, 6, 2249−2257